Smooth Variational Graph Embeddings for Efficient Neural Architecture Search

Jovita Lukasik,[1] **David Friede,** [1] **Arber Zela,**[2]
Heiner Stuckenschmidt, [1] **Frank Hutter,** [2] **Margret Keuper**[1]
[1] University of Mannheim
[2] University of Freiburg
{jovita, david, heiner}@informatik.uni-mannheim.de, keuper@uni.mannheim.de
{zelaa, fh}@cs.uni-freiburg.de

Abstract

In this paper, we propose an approach to neural architecture search (NAS) based on graph embeddings. NAS has been addressed previously using discrete, sampling based methods, which are computationally expensive as well as differentiable approaches, which come at lower costs but enforce stronger constraints on the search space. The proposed approach leverages advantages from both sides by building a smooth variational neural architecture embedding space in which we evaluate a structural subset of architectures at training time using the predicted performance while it allows to extrapolate from this subspace at inference time. We evaluate the proposed approach in the context of two common search spaces, the graph structure defined by the ENAS approach and the NAS-Bench-101 search space, and improve over the state of the art in both.

1 Introduction

Recent progress in computer vision and related domains is to a large extent coupled to the advancement of novel neural architectures (Krizhevsky, Sutskever, and Hinton 2012; Goodfellow et al. 2014). In this context, the automated search of neural architectures (Real et al. 2017; Zoph et al. 2018; Real et al. 2019; Liu et al. 2019; Saikia et al. 2019) becomes increasingly important, as it removes the fatiguing and time-consuming process of manual trial-and-error neural architecture design.

Neural Architecture Search (NAS) is intrinsically a discrete optimization problem and can be solved effectively using black-box methods such as random search (Bergstra and Bengio 2012), reinforcement learning (Zoph and Le 2017; Zoph et al. 2018), evolution (Real et al. 2017; Elsken, Metzen, and Hutter 2018; Real et al. 2019), Bayesian optimization (Kandasamy et al. 2018b; White, Neiswanger, and Savani 2019; Ru et al. 2020) or local search (White, Nolen, and Savani 2020). However, finding a good solution typically requires thousands of function evaluations, which is infeasible without company-scale compute infrastructure. Recent research in NAS focuses more on efficient methods via continuous relaxations of the discrete search space and the weight-sharing paradigm (Bender et al. 2018; Pham et al. 2018; Liu, Simonyan, and Yang 2018; Cai, Zhu, and Han 2019; Xie et al. 2019), but these approaches have their own issues leading to sub-optimal solutions in many cases (Zela et al. 2020). This leads to the desire of an accurate space encoding that enables performance prediction via surrogates and black-box optimization to find high-performing architectures in a continuous search space.

To this end, inspired by the work of Zhang et al. (2019) we propose a smooth variational graph embedding of neural architectures, which can effectively learn to project the directed acyclic graph (DAG) structure of the architectures into a continuous latent space. Our proposed approach extends the method by Li et al. (2018) to build *Smooth Variational Graph embeddings* (SVGes) via a variational autoencoder (Kingma and Welling 2013) that utilizes graph neural networks (GNNs) (Gori, Monfardini, and Scarselli 2005; Kipf and Welling 2016a; Wu et al. 2019) on both its encoder and decoder level. GNNs are a natural choice when it comes to learning on graph-structured data due to their ability to extract local node features and create informative representations of graphs. We show both theoretically and empirically that our proposed SVGe can injectively encode graphs into a continuous latent space and uniquely decodes them back to a discrete representation. This property is essential when encoding neural architectures as graphs since the same topology can be represented by different isomorphic graphs. For robust performance prediction, these should be mapped onto the same latent representation. We show that the extrapolation properties of our generative model, i.e. the ability to accurately represent architectures (graphs) with more nodes than the ones seen during training, can be exploited to find novel, larger architectures with good performance. Finally, by incorporating a triplet loss into the objective, our method is able to capture structural similarities in the neural network architectures and project structurally similar ones close to each other in the variational latent space, facilitating Bayesian optimization.

After discussing related work in Section 2, we make the following contributions:

- We introduce a novel graph variational autoencoder method that builds Smooth Variational Graph embeddings (SVGes) by learning accurate representations of neural architectures in an unsupervised way (Sections 3.1 and 3.2).
- We propose to capture structural relations in graphs and map similar graphs close to one another in the latent space using a triplet loss. We theoretically prove that isomor-

Preprint. Under review.

phic graphs are mapped to the same representation and are uniquely decoded. (Section 3.4)

- We conduct extensive experimental evaluations on the ENAS (Pham et al. 2018) and NAS-Bench-101 (Ying et al. 2019) search spaces and show that optimizing with Bayesian optimization on the latent space achieves on the latter search space a best accuracy of 95.13% outperforming recent methods. (Section 4)

2 Related Work

Graph Generative Models. In recent years the urge for representation learning with Graph Neural Networks (GNNs) of graph-based data increased (Li et al. 2016; Kipf and Welling 2016a; Niepert, Ahmed, and Kutzkov 2016; Hamilton, Ying, and Leskovec 2017). GNNs follow an iterative so called message passing scheme, where node feature vectors aggregate information from their neighbours to update their feature vector (Gilmer et al. 2017), capturing the structural information of neighbours. To obtain a graph-level representation these updated feature vectors are pooled (Ying et al. 2018). GNNs differ in their neighbourhood node information as well as in their graph-level aggregation procedure (Scarselli et al. 2009; Bruna et al. 2013; Henaff, Bruna, and LeCun 2015; Hamilton, Ying, and Leskovec 2017; Kipf and Welling 2016a; Li et al. 2016; Velickovic et al. 2018; Xu et al. 2017, 2018; Verma and Zhang 2018; Ying et al. 2018; Zhang et al. 2018; Xu et al. 2019).

Existing graph generating models can roughly be classified in global approaches and sequential approaches. Global approaches output the full graph at once usually by relaxing the adjacency matrix (Kipf and Welling 2016b; Simonovsky and Komodakis 2018). The sequential approach is an iterative process of adding nodes and edges alternately. Luo et al. (2018) used RNNs to generate neural architectures in this sequential manner. The model in You et al. (2018) introduced a second edge-level RNN capturing the edge dependencies. Zhang et al. (2019) employed an asynchronous message passing scheme instead of RNNs to decode the computations of neural architectures. In contrast, the model in Li et al. (2018) uses the synchronous message passing scheme as known from GNNs for sequential graph generation and expresses superiority over RNNs during the graph generating process. Our model is an extension of the conditional version of Li et al. (2018). The model by Zhang et al. (2019) is also related to our work; unlike our model, it acts on a fixed number of nodes and builds a model on an asynchronous message passing scheme that encodes computations instead of graph structures.

Performance Predictors for Neural Networks. Predicting the performance of neural networks based on features such as the network architecture, training hyperparameters or learning curves has been exploited previously via MCMC methods (Domhan, Springenberg, and Hutter 2015), Bayesian neural networks (Klein et al. 2017) or simple regression models (Baker et al. 2017). Other works such as White, Neiswanger, and Savani (2019) and Long, Zhang, and Zhang (2019) manually construct features to regress simple neural networks or support vector regressors.

More recent work utilizes the GNN encodings by adapting message passing to simulate operations in either edges or nodes in the graph (Ning et al. 2020) or using a semi-supervised approach by training GNNs on relation graphs in the latent space (Tang et al. 2020).

Neural Architecture Search via Bayesian Optimization. The NAS problem can informally be defined as finding an optimal architecture configuration such that it minimizes some validation objective, while that configuration is trained on the training set. Conventional Bayesian optimization (BO) methods cannot be directly used in the popular cell-structured NAS space as it is intrinsically non-continuous and high-dimensional. Kandasamy et al. (2018a) propose to use a distance metric, which they find using an optimal transport program, in order to enable Gaussian process (GP)-based BO. White, Neiswanger, and Savani (2019) focus more on encoding the architecture with a high-dimensional path-based encoding scheme and ensembles of neural networks as surrogate models. Recently, Ru et al. (2020) propose to use a graph kernel with a GP surrogate to naturally handle the graph-like architectures and capture their topological structure. Another line of work utilizes the representations learnt by a GNN in order to fit a Bayesian linear regressor and use that as a surrogate in BO (Shi et al. 2019; Zhang et al. 2019).

Note that we do not introduce any novel BO algorithm, but rather focus on the GNN generative model that learns a smoother latent representation. We use the same strategy as in Zhang et al. (2019) to run BO on this latent space.

3 Structural Graph Autoencoding

Our objective is to learn a continuous latent representation of the topology of neural network architectures, which we cast as directed acyclic graphs (DAGs) with nodes representing operations (like convolution or pooling) and edges representing information flow in the network. This enables to (1) map isomorphic graphs (identical neural architectures) onto the same latent point, (2) accurately predict the accuracy of an unseen graph from few training samples and (3) draw new samples which are structurally similar to previously seen ones.

Our end-to-end model is a *variational autoencoder (VAE)* (Kingma and Welling 2013). Firstly, the encoder $q_\phi(\mathbf{z}|G)$ in the VAE maps the input data G (which consists of a finite number of i.i.d. samples from an unknown distribution) onto a continuous latent variable $\mathbf{z}$ via a parametric function q_ϕ. Then a probabilistic generative model $p_\theta(G|\mathbf{z})$ (the decoder) decodes the latent variables $\mathbf{z}$ back to the original representation. The parameters ϕ and θ of the encoder and decoder, respectively, are optimized by maximizing the evidence lower bound (ELBO):

$$\begin{aligned}\mathcal{L}(\theta, \phi; G) = \mathbb{E}_{q_\phi(\mathbf{z}|G)}\big[\log p_\theta(G|\mathbf{z})\big] \\ - \mathrm{D}_{\mathrm{KL}}(q_\phi(\mathbf{z}|G)\|p(\mathbf{z})),\end{aligned} \tag{1}$$

After the VAE model is trained, new data can be generated by decoding latent space variables $\mathbf{z}$ sampled from the prior distribution $p(\mathbf{z})$.

Below we introduce our encoder (Section 3.1) and decoder (Section 3.2) models for which we employ a graph neural network (GNN). Xu et al. (2019) show that if the GNN function is injective, it maps isomorphic graphs to the same latent point and non-isomorphic graphs to distinct ones. Therefore we select such models for our task. Their expressive capabilities enable to map nodes and graph relations to low-dimensional spaces such as to facilitate neural architecture performance prediction and black-box models such as Bayesian Optimization.

3.1 Encoder

In this section we present our Smooth Variational Graph Embedding (SVGe) encoder which maps from a discrete graph space onto a continuous vector space. As mentioned above, we pick a GNN model (more specifically, the one from Li et al. (2018)) to learn such mapping. Let $G = (V, E)$ be a graph, where V is the set of vertices with $v \in V$ and E the set of edges with $e \in E$. Each node v has an initial node feature embedding $\mathbf{h}_v$. Let $\mathcal{V}^{\text{in}}(v) = \{u \in V \mid (u, v) \in E\}$ be the set of nodes adjacent to $v \in V$. Standard GNNs can be seen as a two-step procedure. In the first step the GNN learns a representation for each node $v \in V$, by iteratively aggregating the representations of the neighbouring nodes and then updating its representation. After K rounds of these iterations, the final representation of each node v is computed. Formally, the first module in the GNN for node aggregation at iteration k is given by

$$\mathbf{a}_v^{(k)} = \mathcal{A}\big(\{\mathbf{h}_u^{(k-1)} : u \in \mathcal{V}(v)\}\big) \tag{2}$$

$$\mathbf{h}_v^{(k)} = \mathcal{U}\big(\mathbf{h}_v^{(k-1)}, \mathbf{a}_v^{(k)}\big), \tag{3}$$

where $\mathbf{h}_v^{(k)}$ is a feature vector representation of node v at iteration k, $\mathcal{A}$ is the node aggregation function and $\mathcal{U}$ is the update function. The second step is the graph-level read-out, where the node representations of the final iteration $\mathbf{h}_v^{(K)}$ are aggregated with the graph-level aggregation function $\tilde{\mathcal{A}}$ to obtain the global graph representation $\mathbf{h}_G$:

$$\mathbf{h}_G = \tilde{\mathcal{A}}\big(\{\mathbf{h}_v^{(K)} \big|\, v \in V\}\big). \tag{4}$$

In our model the aggregation function $\mathcal{A}$ is given by the sum of node message passing modules $\mathbf{m}_{u\to v} = f_n(\mathbf{h}_u, \mathbf{h}_v) = \text{MLP}(\text{concat}(\mathbf{h}_u, \mathbf{h}_v)$. This message passing module computes a message vector from node u to node v. To capture the overall structure of the graphs, we also consider the reverse message passing module $\mathbf{m}_{v\to u} = \hat{f}_n(\mathbf{h}_v, \mathbf{h}_u) = \widehat{\text{MLP}}(\text{concat}(\mathbf{h}_u, \mathbf{h}_v)$, which leads to a bidirectional message passing, yielding the global aggregation

$$a_v^{(k)} = \sum_{u\in\mathcal{V}^{\text{in}}} f_n(\mathbf{h}_u, \mathbf{h}_v) + \sum_{u\in\mathcal{V}^{\text{out}}} \widehat{f}_n(\mathbf{h}_v, \mathbf{h}_u), \tag{5}$$

where $\mathcal{V}^{\text{out}}(v) = \{u \in V \mid (v, u) \in E\}$. Furthermore, we use a learnable look-up table L_e on the node types for our initial node embeddings $\mathbf{h}_v$. As for the update function $\mathcal{U}$, we utilize a single gated recurrent unit (GRU) (Chung et al. 2014). For the graph-level aggregation after the final round of message passing, we aggregate the node embeddings $(\mathbf{h}_v^{(K)})_{v\in V}$ into a single graph representation using a gated sum:

$$\mathbf{h}_G = \sum_{v\in V} g(\mathbf{h}_v^{(K)}) \odot f_g(\mathbf{h}_v^{(K)}), \tag{6}$$

where $g = \sigma(\text{MLP}(\cdot))$, is a gating network and f_g a multilayer perceptron (MLP), $\odot$ being the Hadamard product. Note that, since we use this encoder in a variational autoencoder setting, we add an extra graph aggregation layer equal to (6) to obtain $\mathbf{h}_G^{\text{var}}$. Thus, the outputs of our encoder are the parameters of the approximate posterior distribution function $q_\phi = \mathcal{N}(\mathbf{h}_G, \mathbf{\Sigma})$, with $\mathbf{h}_G$ being the mean and $\mathbf{h}_G^{\text{var}}$ the diagonal of the variance-covariance matrix $\mathbf{\Sigma}$ of the multivariate normal distribution. See Section 3.4 for a detailed discussion on the properties of the encoder w.r.t. injectivity and isomorphic graphs.

3.2 Decoder

The decoder $p_\theta(G|\mathbf{z})$ takes a sampled point $\mathbf{z}$, which encodes in a low-dimensional continuous representation the original graph G, from the latent space $q_\phi(\mathbf{z}|G)$ as input and generates a graph iteratively as a sequence of operations that add new nodes and edges until the end/output node is generated.

Graph Generation. Our decoder consists of multiple modules to define a distribution over the outputs in each iteration in the generation process. In each iteration t at least one of the following inputs is used:

$\mathbf{z}$	a sampled point from $q_\phi(\mathbf{z}\|G)$,
L_d	a look-up table based on the node types,
$\mathbf{h}_t$	the embedding of the created node $v_t \in \tilde{V}$,
$\tilde{G}^{(t)}, \mathbf{h}_{\tilde{G}^{(t)}}$	the partial graph and its embedding.

Note that the learnable embedding look-up table L_d is independent of the one in Section 3.1. We begin the iteration with the initial input node, which is initialized according to the sampled point $\mathbf{z}$ and the look-up table L_d yielding in an initial node embedding $\mathbf{h}_0$. Afterwards, we can represent the full graph generating process by iterating over the following modules. Note that the modules' weights are shared across different iterations.

Prop. Firstly, this module aggregates and updates the initial node embeddings $\mathbf{h}_{\tilde{V}}$ for all nodes $v_t \in \tilde{V}$ in the partial graph $\tilde{G}^{(t)} = (\tilde{V}, \tilde{E})$ based on the look-up table L_d. Then, the updated node embeddings are read-out and aggregated into a single graph representation $\mathbf{h}_{\tilde{G}^{(t)}}$:

$$(\mathbf{h}_{\tilde{G}^{(t)}}, \mathbf{h}_{\tilde{V}^{(t)}}) = f_{\text{prop}}(\mathbf{h}_{\tilde{V}}, \tilde{G}^{(t)}). \tag{7}$$

This module is exactly the encoder introduced in Section 3.1, (5) - (6), initialized with its own weights. This idea of using two distinct GNNs on the encoder and decoder level is motivated by NLP methods, which use ordinary RNNs (Bowman et al. 2016; Sutskever, Vinyals, and Le 2014).

AddNode. In this module a new node is created and its node type (i.e. operation in the network architecture case) is selected. The input for this module is the updated graph

representation of the already created partial graph $\mathbf{h}_{\tilde{G}^{(t)}}$, created by the *prop* module, and the sampled point $\mathbf{z}$, which is a summary of the input graph given to the encoder. The intention behind using both these inputs is based on the idea of comparing the partial graph with the true graph in order to find the missing pieces and thus recreating the desired graph. This yields the following module:

$$\text{NodeType} \sim \text{Categorical}(s^{(t+1)}_{\text{addNode}}), \tag{8}$$

where

$$s^{(t+1)}_{\text{addNode}} = f_{\text{addNode}}(\mathbf{z}, \mathbf{h}_{\tilde{G}^{(t)}}) \tag{9}$$

The *addNode* module first produces parameters for the node type distribution. Secondly, we sample from this categorical distribution over all possible node types yielding a one-hot encoding of a specific node type. Since we aim to generate graphs representing neural architectures, the iteration stops after running through the step that adds the output node in the DAG.

InitNode. When a new node is added with the *addNode* module, we need to initialize its node embedding:

$$\mathbf{h}_{t+1} = f_{\text{initNode}}(\mathbf{z}, \mathbf{h}_{\tilde{G}^{(t)}}, \text{L}_\text{d}[\text{type}]), \tag{10}$$

where the input is the sampled point $\mathbf{z}$, the partial graph embedding $\mathbf{h}_{\tilde{G}^{(t)}}$ and the node embedding based on the look-up table $\text{L}_\text{d}[\text{type}]$. Furthermore this new node embedding is then added to the already existing propagated node embedding, $\mathbf{h}_{\tilde{V}} = \text{concat}((\mathbf{h}_j)_{0 \le j \le t}, \mathbf{h}_{t+1})$.

AddEdges. This module selects the edges towards the newly created node. For this purpose we calculate scores for an edge between the new node v_{t+1} and each previous node. A high score stands for a high probability. This module takes all partial graph node embeddings as input, as well as the partial graph embedding $\mathbf{h}_{\tilde{G}^{(t)}}$ and the sampled point $\mathbf{z}$, leading to

$$e_{(i,t+1)} \sim \text{Bernoulli}(s^{(i,t+1)}_{\text{addEdges}}), \tag{11}$$

where

$$s^{(i,t+1)}_{\text{addEdges}} = f_{\text{addEdges}}(\mathbf{h}_{t+1}, \mathbf{h}_{\tilde{V} \setminus v_{t+1}}, \mathbf{h}_{\tilde{G}^{(t)}}, \mathbf{z}). \tag{12}$$

The calculated score $s^{(i,t+1)}_{\text{addEdges}}$ for each possible edge is then passed into a Bernoulli distribution over the possible edges. Sampling from this distribution yields the new set of edges. Since we want to generate DAGs, we interpret each edge as directed towards the new node. Unless stated otherwise, in all our experiments we set f_{addNode}, f_{initNode} and f_{addEdges} as two-layer MLPs with ReLU non-linearities.

See Algorithm 1 for an overview of our DAG decoder.

Algorithm 1: Graph Generation

Input: embedding $\mathbf{z}$ of graph $G = (V, E)$, L_d look-up table for node types
Output: reconstructed graph $\tilde{G} = (\tilde{V}, \tilde{E})$

initialize $v_0 \leftarrow$ InputNode with type (v_0)$\leftarrow$ InputType and its embedding L_d[InputType]
$\mathbf{h}_0 \leftarrow f_{\text{initNode}}(\mathbf{z}, \text{L}_\text{d}[\text{InputType}])$; ▷ Eq. (10)
$\tilde{V} \leftarrow \{v_0\}$, $\tilde{E} \leftarrow \emptyset$
$\mathbf{h}_{\tilde{G}} \leftarrow \tilde{\mathbf{z}} \sim q_\phi(\tilde{\mathbf{z}}|\tilde{G})$, $\mathbf{h} = [\mathbf{h}_0]$
$v_t \leftarrow v_0$, $\mathbf{h}_t \leftarrow \mathbf{h}_0$
while type(v_t) $\neq$ EndingType **do**
  $\tilde{V} \leftarrow \tilde{V} \cup \{v_{t+1}\}$; ▷ add node
  $s_{\text{addNode}} \leftarrow f_{\text{addNode}}(\mathbf{z}, \mathbf{h}_{\tilde{G}})$; ▷ Eq. (9)
  type(v_{t+1}) $\sim$ Categorical(s_{addNode}) ; ▷ get type (8)
  $\mathbf{h}_{t+1} \leftarrow f_{\text{initNode}}(\mathbf{z}, \mathbf{h}_{\tilde{G}}, \text{L}_\text{d}[\text{type}(v_{t+1})])$; ▷ Eq. (10)
  for $v_j \in \tilde{V} \setminus v_{t+1}$ **do**
    $s_{\text{addEdges}}(j, t+1) \leftarrow f_{\text{addEdges}}(\mathbf{h}_{t+1}, \mathbf{h}, \mathbf{h}_{\tilde{G}}, \mathbf{z})$; ▷ Eq. (12)
    $e_{(j,t+1)} \sim \text{Ber}(s_{\text{addEdges}}(j, t+1))$; ▷ sample whether to add edge, Eq. (11)
    if $e_{(j,t+1)} = 1$ **then**
      $\tilde{E} \leftarrow \tilde{E} \cup \{e_{(j,t+1)} = (v_j, v_{t+1})\}$; ▷ add edge
    end
  end
  $\mathbf{h} \leftarrow \text{concat}(\mathbf{h}, \mathbf{h}_{t+1})$
  $(\mathbf{h}, \mathbf{h}_{\tilde{G}}) \leftarrow f_{\text{prop}}(\mathbf{h}, \tilde{G})$; ▷ update node embeddings and reconstructed graph embedding, Eq. (7)
  $t \leftarrow t + 1$
end

3.3 Loss Function and Training

As shown in equation 1, VAE maximizes the evidence lower bound (ELBO), where the first term is the reconstruction loss which enforces high similarity between the input graph and the generated graph, while the second term is the Kullback–Leibler divergence which regularizes the latent space. In the following, we will discuss the reconstruction loss of SVGe. We train the encoder and the decoder of SVGe jointly in an unsupervised manner. Given a fixed node ordering of the DAG, which we discuss in Section 3.4, we know the ground truth of the outputs of *AddNode* (equation 8) and *AddEdges* (equation 11) during training. On the one hand, we can use this ground truth to compute a node-level loss $\mathcal{L}^t_V$ and an edge-level loss $\mathcal{L}^t_E$ at each iteration t. On the other hand, we can replace the model output by the ground truth such that possible errors will not accumulate throughout iterations. This is also known as teacher forcing (Williams and Zipser 1989).

To compute the overall reconstruction loss for a graph G, we sum up node losses and edge losses over all iterations:

$$\mathcal{L}_{rec} = \mathcal{L}_V + \mathcal{L}_E. \tag{13}$$

Following Kingma and Welling (2013), we assume $p_\theta(\mathbf{z}) \sim \mathcal{N}(\mathbf{z}; \mathbf{0}, \mathbb{1})$ and $p_\theta(G|\mathbf{z}) \sim \mathcal{N}(\mathbf{h}_G, \mathbf{\Sigma})$. Furthermore, we approximate the posterior by a multivariate Gaussian distribution with diagonal covariance structure. This can be written as $\log q_\phi(\mathbf{z}|G) = \log \mathcal{N}(\mathbf{z}; \mathbf{h}_G, \mathbf{\Sigma})$ and en-

sures a closed form of the KL divergence

$$\mathrm{D}_{\mathrm{KL}} = -\frac{1}{2}\sum_{j=1}^{J}\left(1+\log(\mathbf{h}_G^{\mathrm{var}})_j - (\mathbf{h}_G)_j^2 - (\mathbf{h}_G^{\mathrm{var}})_j\right). \quad (14)$$

Thus, the overall loss function is

$$\mathcal{L} = \mathcal{L}_V + \mathcal{L}_E + \alpha \mathrm{D}_{\mathrm{KL}}, \quad (15)$$

where the KL divergence is additionally regularized. Following Jin, Barzilay, and Jaakkola (2018) and Zhang et al. (2019), we set $\alpha = 0.005$.

Triplet Loss. While the proposed variational graph autoencoder is encouraged to create an efficient latent space representation in which similar graphs are close to one another, there is no guarantee nor explicit loss forcing it to actually do so. Specifically, depending on the size of the latent embedding, the encoder might choose to create efficient subspace representations for some sub-graphs and map graphs at random in other latent dimensions. Therefore, we propose to employ a triplet loss formulated on the graph structure with the aim to ensure that structurally similar graphs are closer to one another than structurally dissimilar graphs in their latent representation.

We measure the distance between two graphs as the edit distance d_κ, which is the smallest number of changes that are required to transform one graph into another; one change consists in either turning an operation, i.e. the node's label, or adding and removing an edge, respectively. We include graph triplets $\mathbf{G_t}$ in the input to our graph autoencoder. Each triplet $\mathbf{G_t}$ consists of an anchor graph G_i, which is also used for the generative model as input graph, a "positive" graph G_j, for which $d_\kappa(G_i, G_j) < \varepsilon$ holds, and a "negative" graph G_k with the property $d_\kappa(G_i, G_k) > \delta$, which we map onto a latent space via the posterior $q_\phi(\mathbf{z}|G)$. Our aim is to adapt the latent space, which is done by introducing a triplet loss of the embeddings of the triplet graphs. For each graph G_i, G_j, G_k we sample its latent variables from the corresponding posterior $\mathbf{t}_{i,j,k} \sim q_\phi(\mathbf{t}|G_{i,j,k})$ in order to calculate the triplet loss

$$\mathcal{L}_{TL_\phi}(\mathbf{t}|G_i, G_j, G_k) = \left(\|t_i - t_j)\|^2 - \|t_i - t_k\|^2 + \alpha\right)_+ \quad (16)$$

with $\|\cdot\|$ being the Euclidean distance and $(x)_+ := \max(x, 0)$. For our proposed SVGe triplet model the overall loss is then given by a convex combination:

$$\begin{aligned}\mathcal{L}(\theta, \phi; G_i, G_j, G_k) = \lambda\big(&\mathbb{E}_{q_\phi(\mathbf{z}|G_i)}\left[\log p_\theta(G_i|\mathbf{z})\right] \\ &- \mathrm{D}_{\mathrm{KL}}(q_\phi(\mathbf{z}|G_i)\|p(\mathbf{z}))\big) \\ &+ (1-\lambda)\big(\mathcal{L}_{TL_\phi}(\mathbf{t}|G_i, G_jG_k)\big)\end{aligned} \quad (17)$$

The λ balances the influence of the actual VAE loss and the triplet loss in the overall model loss. Karaletsos, Belongie, and Rätsch (2016) use a similar approach, with the difference that they include triplets from an oracle into the VAE framework in order to find a mapping which captures dependencies between these triplets and some observations. Our goal is an adaptation of the embedding space which captures the structural closeness and dependencies of the graphs G.

3.4 Discussion

To study the graph representation and generation power of our SVGe, we first analyse the ability of our encoder to map two non-isomorphic graphs to different embedding space points as well as mapping isomorphic graphs to the same one. Then we discuss the ability of our decoder to decode isomorphic graphs and non-isomorphic graphs uniquely.

Unique embeddings of neural architectures into a low-dimensional space are in particular relevant for any performance prediction model utilizing the latent representation. These performance prediction models can eventually be used as surrogate models in black-box optimization (White, Neiswanger, and Savani 2019; Zhang et al. 2019; Shi et al. 2019; Siems et al. 2020). If two non-isomorphic graphs with very different performances were mapped to the same representation in the latent space, the loss at this ground truth performance would not be well defined hindering the model training process. Conversely, if two isomorphic graphs which have by definition the same performance, are mapped to two different embeddings in the latent space, a performance prediction model would interpret these equal graphs as different ones. This prevents the efficient embedding of structural similarity.

Unique Latent Space Representation. Following the above discussion, we discuss the suitability of the proposed GNN encoder w.r.t. mapping any two different (non-isomorphic) graphs to different encodings in the latent space and to learn to map isomorphic graphs to the same encoding.

Theorem 3 in Xu et al. (2019) states that if the GNN's node aggregation module $\mathcal{A}$ and its update module $\mathcal{U}$ are injective, and the graph-level readout aggregation is injective on the multiset $\mathbf{h}_v^{(k)}$, the GNN maps any two non-isomorphic graphs to different embeddings. With our choice of aggregation modules for the node level features and for the graph-level read-out and of the update module, we fulfil the criteria in *Theorem 3*. This property enables robust performance prediction out of the embedding space, which can be crucial for many NAS algorithms (Liu, Simonyan, and Yang 2018; White, Neiswanger, and Savani 2019; Zhang et al. 2019).

Decoding from the Latent Space. We now discuss how the decoder handles isomorphic DAGs in a suitable way.

Proposition 1. *Let G_1, G_2 be two isomorphic graphs representing neural networks. Let furthermore the encoder be able to injectively encode isomorphic graphs to the same latent point.*

Given the input node v_0 in the DAG and a sampled point in the latent space $\mathbf{z}$, the SVGe decoder decodes isomorphic graphs to the same output.

One obvious question arises: what does the decoder do at training time, when it has to learn to decode two isomorphic graphs, having the same multivariate Normal distribution as an input? Learning to decode graph G_1 instead of any isomorphic graph G_2 leads to a loss at training time. To keep this loss as small as possible, the decoder needs a certain node ordering in the training signal. Since the decoder decodes the graphs in a sequential manner the order is restricted to be an upper triangular adjacency matrix.

Proposition 2. *Every isomorphy class S_n of graphs contains at least of one graph whose adjacency matrix is in upper triangular form.*

The proofs of both propositions can be found in the appendix C. It follows from proposition 2, that the set of isomorphic upper triangular matrices is a subset of the isomorphy class S_n itself. Eventually, we only need to consider that subset. Here is it worth discussing if we can bound this subset. To remove as many possible isomorphic graphs from the training set as possible, we bring the graphs in a unified form by transforming them into an upper triangular matrix such that they can be built in a sequential manner. Specifically, nodes in the adjacency matrix are ordered such that every node is connected to at least one preceding node. The number of such graphs, including isomorphic graphs, can be upper bounded to $\sum_{k=1}^{n} 2^{k-1} - 1$. The remaining isomorphic graphs are removed from the training set by the method used in Ying et al. (2019).

As described in Section 3.2 the SVGe decoder generates node v_i and connects it to previous nodes $v_j, j < i$ with an edge (j, i). Thus, the decoder builds such an upper triangular adjacency matrix, which is filled column-wise.

4 Experiments

We pick 2 different search spaces from the NAS literature and run our SVGe model to learn a latent representation of the architectures sampled from those spaces.

NAS-Bench-101. NAS-Bench-101 (Ying et al. 2019) is a tabular benchmark that consists of cell-structured search space containing 423k unique architectures evaluated for $4, 12, 36$ and 108 epochs on the CIFAR-10 classification task. The cell structure is limited to a number of nodes $|V| \leq 7$ (including the input and output node) and edges $|E| \leq 9$. The nodes represent an operation from the operation set $\mathcal{O} = \{1 \times 1 \text{ convolution}, 3 \times 3 \text{ convolution}, 3 \times 3 \text{ max pooling}\}$. In our experiments, we use 90% of the 423k $(\text{architecture}, \text{accuracy})$ pairs as training examples and 10% as validation ones.

ENAS search space. The ENAS (Pham et al. 2018) search space consists of architectures represented by a DAG with $|V| = 8$ nodes (including the input and output node) and 6 operation choices on each of the non-input and non-output nodes. The total number of sampled architectures we utilize from this space $19,020$ (as in Zhang et al. (2019)). Differently from the NAS-Bench-101 benchmark, which contains the true performance of the fully trained architectures, here we utilize the weights of the optimized one-shot model as a proxy for the validation/test performance of the sampled architectures. Again, we split the $(\text{architecture}, \text{accuracy})$ pairs into 90% training and 10% testing examples.

More details on both search spaces are given in the appendix A. We conduct experiments on three complementary tasks and in the appendix D we provide a further analysis of other basic abilities of the SVGe and SVGe triplet models. In all our experiments, we set $\mathbf{h}_v \in \mathbb{R}^{250}$ for the node dimension and $\mathbf{h}_G \in \mathbb{R}^{56}$ for the latent space dimension. Training details are given in appendix B. All the algorithms and routines are implemented using PyTorch (Paszke et al. 2017) and PyTorch Geometric (Fey and Lenssen 2019).

4.1 Performance Prediction from Latent Space

In the following, we evaluate the smooth embedding space generated by our SVGe and SVGe triplet model to accurately predict performances of NAS-Bench-101 architectures, which allows direct comparison to the contemporary work Tang et al. (2020). Concretely, we train the SVGe on all 423k datapoints for reconstruction to obtain the latent space. The triplets are generated by setting $\varepsilon = 3$ and $\delta = 4$ and we sample in total 38k (10%) triplets out of the training set to train the SVGe triplet model for graph reconstruction. Then, we fine-tune the unsupervisedly trained model for performance prediction using a regressor, which is a four-layer MLP with ReLU non-linearities. Both the SVGe model and the regressor are trained jointly for performance prediction on 1k randomly sampled architectures and their test accuracies queried from NAS-Bench-101.

Firstly, we compare the ability to predict performances accurately on the validation set. In table 1 (*left*) we show the mean MSE, which denotes the empirical squared loss between the predicted and ground truth data, and relative standard deviation of 3 runs. Our proposed SVGe triplet has a slightly better mean MSE compared to the method in Tang et al. (2020), which focuses precisely on this subproblem, when a small amount of annotated data is given. This is important in particular for NAS, since every training sample corresponds to a fully evaluated architecture and is thus expensive to evaluate.

Next, we analyse the ability of the proposed SVGe to find high-performing neural architectures in the validation set. For that we train the SVGe model jointly with the regressor using 3k random samples of labelled data. The true best neural architecture in this validation set achieves a test accuracy of 94.22%, which is comparable to the values in Tang et al. (2020), whose true best neural architecture has a test accuracy of 94.23%. Table 1 (right) shows the result of the best found architecture and their ranking within our validation set. The best network found by SVGe has a true test accuracy of 94.10%, which is within the best 0.01% architectures, outperforming the proposed method from Tang et al. (2020). As soon as we have enough labelled data for the performance prediction task, the triplet loss does not further improve the interpolation ability.

4.2 Extrapolation Ability

To validate the search of neural architectures with high performance out of the embedding space, we exploit in this section the ability of our generative model to extrapolate from the labelled dataset, i.e. the ability to predict neural architectures with high performance on the CIFAR-10 classification task with more nodes and edges than seen at training time in both NAS-Bench-101 and ENAS search spaces.

We start with the extrapolation task on the NAS-Bench-101 search space, where we generate graphs (cells) containing 8 and 9 nodes. Note that our SVGe model has never seen during training these types of architectures since NAS-Bench-101 contains only architectures with cells up to 7

Surrogate-Model	Performance Prediction			Test Accuracies (in %)	
	$1,000$	$10,000$	$100,000$	Top-1 Acc.	Ranking
Semi-Superv. Ass.(Tang et al. 2020)	0.0031	0.0026	$\mathbf{0.0016}$	94.01	0.03
SVGe	0.0037 ± 0.007	0.0025 ± 0.006	0.0021 ± 0.1079	$\mathbf{94.10}$	$\mathbf{0.01}$
SVGe Triplet	$\mathbf{0.003 \pm 0.078}$	$\mathbf{0.0023 \pm 0.009}$	0.0021 ± 0.0100	94.10	0.01

Table 1: Comparison of predictive performance of surrogate models in terms of MSE and the relative standard deviation on the test accuracies of NAS-Bench-101 (left). Test accuracies on the CIFAR-10 classification task. 3k randomly sampled architectures from NAS-Bench-101 are used for fine-tuning (right).

Dataset	Method	Top-1 Acc. (%)	Top-5 Acc. (%)
NB101-7	*oracle*	95.15	-
NB101-8	SVGe	$\mathbf{95.18}$	$\mathbf{95.21}$
NB101-9	SVGe	94.71	95.15
ENAS-12	D-VAE	96.12	-
	SVGe	$\mathbf{96.15}$	$\mathbf{96.15}$

Table 2: Validation accuracies for architecture extrapolation on NAS-Bench-101 and the ENAS search space.

nodes and no more than that. To generate these new graphs we firstly pick the best performing graph from NAS-Bench-101 based on the validation accuracy and expand it to graphs with 8 and 9 nodes. Next, we randomly generate the upper triangular matrices considering the new node length. The total number of sampled graphs is 3k and out of these we select the best 5 based on the predicted validation accuracy (see section 4.1). These best models are finally trained from scratch on CIFAR-10 using the exact training pipeline as in Ying et al. (2019). As we can see from the top 3 rows in Table 2, the architectures found by extrapolating using our SVGe model achieve a top-1 validation accuracy of 95.18% for graphs of length 8, which is comparable to the best 7-node architecture accuracy (95.15%). The lower validation accuracy (94.71%) of the architecture with 9 nodes is not surprising since we are using the exact training settings which were tuned for the 7-node case.

On the ENAS search space, we evaluated our SVGe on the macro architecture containing a total of 12 nodes (layers) compared to architectures with 8 nodes used during the SVGe training. We further fine-tune the embedding space by sampling 1k architectures from the training set and train the SVGe together with the performance predictor jointly. Note that the performance predictor here uses the weight-sharing accuracies as proxy for the true accuracy of the fully trained architectures. We select top 5 architectures based on the predicted validation performance and again fully train them on CIFAR-10, using the exact settings as in Zhang et al. (2019). As shown in table 2, the best found architecture in the ENAS search space achieves a validation accuracy of 96.15% which is close to the one found by extrapolating using the model in (Zhang et al. 2019), but the runtime required to evaluate the embedding space is faster by factor 3.

Dataset	Method	Top-1 Acc. (%)	Runtime (GPU h)
ENAS	D-VAE	94.80	16
	SVGe	95.04	$\mathbf{5}$
	SVGe Triplet	$\mathbf{95.13}$	10

Table 3: Bayesian optimization on the ENAS Search Space. Both our embeddings outperform the recent method D-VAE and reduce the runtime required to evaluate the embedding space by a factor up to 3.

4.3 Bayesian Optimization

We have seen in the previous experiments that our proposed SVGe generates a latent space which enables to interpolate and extrapolate from seen labels/performances. Next, we perform NAS via Bayesian optimization (BO) in the generated continuous ENAS search space, in order to have a fair comparison to D-VAE (Zhang et al. 2019) by changing only the D-VAE generative model with our SVGe and using exactly the same setup as in Zhang et al. (2019).

Following Zhang et al. (2019) and Kusner, Paige, and Hernández-Lobato (2017) we perform 10 iterations of batch BO (with a batch size of 50) and average the results across 10 trials based on a Sparse Gaussian Process (SGP) (Snelson and Ghahramani 2005) with 500 inducing points and expected improvement (EI) (Mockus 1974) as acquisition function. We select the best 15 architectures w.r.t. their weight-sharing accuracies and fully train them from scratch on CIFAR-10, as done in (Zhang et al. 2019). As we can see in Table 3, SVGe's best found architecture achieves an accuracy of 95.04%. Using SVGe with triplet loss enables finding an architecture with 95.13% test accuracy, which is 0.33 percentage points better than the best found architecture using the D-VAE learned embedding. BO on NAS-Bench-101 yields a well performing architecture with accuracy of 94.73% (i.e. on par with D-VAE on ENAS).

5 Conclusion

In this paper, we proposed SVGe and SVGe triplet, a Smooth Variational Graph embedding model for NAS. We give theoretical results on SVGe about injectively encoding properties and uniquely decoding abilities of graph-structured data. We present results on the NAS-Bench-101 and the ENAS search spaces and show improvements over state of the art approaches for performance prediction surrogate models and Bayesian optimization in the smooth embedding space.

Acknowledgement

The authors acknowledge support by the German Federal Ministry of Education and Research Foundation via the project DeToL.

References

Baker, B.; Gupta, O.; Naik, N.; and Raskar, R. 2017. Designing Neural Network Architectures using Reinforcement Learning. *ICLR* .

Bender, G.; Kindermans, P.-J.; Zoph, B.; Vasudevan, V.; and Le, Q. 2018. Understanding and Simplifying One-Shot Architecture Search. In *ICML*.

Bergstra, J.; and Bengio, Y. 2012. Random Search for Hyper-Parameter Optimization. *Journal of Machine Learning Research* 13(10): 281–305.

Bowman, S. R.; Vilnis, L.; Vinyals, O.; Dai, A. M.; Józefowicz, R.; and Bengio, S. 2016. Generating Sentences from a Continuous Space. In *Conference on Computational Natural Language Learning,*, 10–21.

Bruna, J.; Zaremba, W.; Szlam, A.; and LeCun, Y. 2013. Spectral networks and locally connected networks on graphs. *arXiv preprint arXiv:1312.6203* .

Cai, H.; Zhu, L.; and Han, S. 2019. ProxylessNAS: Direct Neural Architecture Search on Target Task and Hardware. In *ICLR*.

Chung, J.; Gulcehre, C.; Cho, K.; and Bengio, Y. 2014. Empirical evaluation of gated recurrent neural networks on sequence modeling. In *NIPS 2014 Workshop on Deep Learning, December 2014*.

Domhan, T.; Springenberg, J. T.; and Hutter, F. 2015. Speeding Up Automatic Hyperparameter Optimization of Deep Neural Networks by Extrapolation of Learning Curves. In *IJCAI*, 3460–3468.

Elsken, T.; Metzen, J. H.; and Hutter, F. 2018. Neural architecture search: A survey. *arXiv preprint arXiv:1808.05377* .

Falkner, S.; Klein, A.; and Hutter, F. 2018. BOHB: Robust and Efficient Hyperparameter Optimization at Scale. In Dy, J.; and Krause, A., eds., *Proceedings of the 35th International Conference on Machine Learning*, volume 80 of *Proceedings of Machine Learning Research*, 1437–1446. PMLR.

Fey, M.; and Lenssen, J. E. 2019. Fast graph representation learning with PyTorch Geometric. *arXiv preprint arXiv:1903.02428* .

Gilmer, J.; Schoenholz, S. S.; Riley, P. F.; Vinyals, O.; and Dahl, G. E. 2017. Neural message passing for quantum chemistry. In *ICML*, 1263–1272. JMLR. org.

Goodfellow, I.; Pouget-Abadie, J.; Mirza, M.; Xu, B.; Warde-Farley, D.; Ozair, S.; Courville, A.; and Bengio, Y. 2014. Generative adversarial nets. In *Advances in neural information processing systems*, 2672–2680.

Gori, M.; Monfardini, G.; and Scarselli, F. 2005. A new model for learning in graph domains. In *Proceedings. 2005 IEEE International Joint Conference on Neural Networks, 2005.*, volume 2, 729–734. IEEE.

Hamilton, W.; Ying, Z.; and Leskovec, J. 2017. Inductive representation learning on large graphs. In *Advances in Neural Information Processing Systems*, 1024–1034.

He, K.; Zhang, X.; Ren, S.; and Sun, J. 2016. Deep residual learning for image recognition. In *CVPR*.

Henaff, M.; Bruna, J.; and LeCun, Y. 2015. Deep convolutional networks on graph-structured data. *arXiv preprint arXiv:1506.05163* .

Jin, W.; Barzilay, R.; and Jaakkola, T. S. 2018. Junction Tree Variational Autoencoder for Molecular Graph Generation. In *ICML*, 2328–2337.

Kandasamy, K.; Neiswanger, W.; Schneider, J.; Poczos, B.; and Xing, E. 2018a. Neural Architecture Search with Bayesian Optimisation and Optimal Transport. In *NeurIPS*.

Kandasamy, K.; Neiswanger, W.; Schneider, J.; Póczos, B.; and Xing, E. P. 2018b. Neural Architecture Search with Bayesian Optimisation and Optimal Transport. In *Advances in Neural Information Processing Systems*, 2020–2029.

Karaletsos, T.; Belongie, S. J.; and Rätsch, G. 2016. When crowds hold privileges: Bayesian unsupervised representation learning with oracle constraints. In Bengio, Y.; and LeCun, Y., eds., *ICLR*.

Kingma, D. P.; and Ba, J. 2015. Adam: A Method for Stochastic Optimization. In *ICLR*.

Kingma, D. P.; and Welling, M. 2013. Auto-encoding variational bayes. *arXiv preprint arXiv:1312.6114* .

Kipf, T. N.; and Welling, M. 2016a. Semi-supervised classification with graph convolutional networks. *arXiv preprint arXiv:1609.02907* .

Kipf, T. N.; and Welling, M. 2016b. Variational graph auto-encoders. *arXiv preprint arXiv:1611.07308* .

Klein, A.; Falkner, S.; Springenberg, J. T.; and Hutter, F. 2017. Learning Curve Prediction with Bayesian Neural Networks. In *ICLR*.

Krizhevsky, A. 2009. Learning multiple layers of features from tiny images. Technical report, University of Toronto.

Krizhevsky, A.; Sutskever, I.; and Hinton, G. E. 2012. Imagenet classification with deep convolutional neural networks. In *Advances in neural information processing systems*, 1097–1105.

Kusner, M. J.; Paige, B.; and Hernández-Lobato, J. M. 2017. Grammar Variational Autoencoder. In Precup, D.; and Teh, Y. W., eds., *ICML*, volume 70 of *Proceedings of Machine Learning Research*, 1945–1954.

Li, Y.; Tarlow, D.; Brockschmidt, M.; and Zemel, R. S. 2016. Gated Graph Sequence Neural Networks. In Bengio, Y.; and LeCun, Y., eds., *ICLR*.

Li, Y.; Vinyals, O.; Dyer, C.; Pascanu, R.; and Battaglia, P. W. 2018. Learning Deep Generative Models of Graphs. *CoRR* abs/1803.03324.

Liu, C.; Chen, L.; Schroff, F.; Adam, H.; Hua, W.; Yuille, A. L.; and Li, F. 2019. Auto-DeepLab: Hierarchical Neural Architecture Search for Semantic Image Segmentation. In *CVPR*, 82–92. Computer Vision Foundation / IEEE.

Liu, H.; Simonyan, K.; and Yang, Y. 2018. DARTS: Differentiable Architecture Search. *CoRR* abs/1806.09055. URL http://arxiv.org/abs/1806.09055.

Long, D.; Zhang, S.; and Zhang, Y. 2019. Performance Prediction Based on Neural Architecture Features. *2019 2nd China Symposium on Cognitive Computing and Hybrid Intelligence (CCHI)* 77–80.

Luo, R.; Tian, F.; Qin, T.; Chen, E.; and Liu, T.-Y. 2018. Neural architecture optimization. In *Advances in neural information processing systems*, 7816–7827.

Mockus, J. 1974. On Bayesian Methods for Seeking the Extremum. In Marchuk, G. I., ed., *Optimization Techniques, IFIP Technical Conference, Novosibirsk, USSR*, volume 27 of *Lecture Notes in Computer Science*, 400–404. Springer.

Niepert, M.; Ahmed, M.; and Kutzkov, K. 2016. Learning convolutional neural networks for graphs. In *ICML*, 2014–2023.

Ning, X.; Zheng, Y.; Zhao, T.; Wang, Y.; and Yang, H. 2020. A Generic Graph-based Neural Architecture Encoding Scheme for Predictor-based NAS. *CoRR* abs/2004.01899.

Paszke, A.; Gross, S.; Chintala, S.; Chanan, G.; Yang, E.; DeVito, Z.; Lin, Z.; Desmaison, A.; Antiga, L.; and Lerer, A. 2017. Automatic Differentiation in PyTorch. In *NIPS Autodiff Workshop*.

Pham, H.; Guan, M. Y.; Zoph, B.; Le, Q. V.; and Dean, J. 2018. Efficient Neural Architecture Search via Parameter Sharing. In *ICML*, 4092–4101.

Real, E.; Aggarwal, A.; Huang, Y.; and Le, Q. V. 2019. Regularized Evolution for Image Classifier Architecture Search. In *The Thirty-Third AAAI Conference on Artificial Intelligence, AAAI*, 4780–4789. AAAI Press.

Real, E.; Moore, S.; Selle, A.; Saxena, S.; Suematsu, Y. L.; Tan, J.; Le, Q. V.; and Kurakin, A. 2017. Large-Scale Evolution of Image Classifiers. In *ICML*, 2902–2911.

Ru, B.; Wan, X.; Dong, X.; and Osborne, M. 2020. Neural Architecture Search using Bayesian Optimisation with Weisfeiler-Lehman Kernel. *ArXiv* abs/2006.07556.

Saikia, T.; Marrakchi, Y.; Zela, A.; Hutter, F.; and Brox, T. 2019. AutoDispNet: Improving Disparity Estimation With AutoML. In *2019 IEEE/CVF International Conference on Computer Vision, ICCV*, 1812–1823. IEEE.

Scarselli, F.; Gori, M.; Tsoi, A. C.; Hagenbuchner, M.; and Monfardini, G. 2009. The Graph Neural Network Model. *IEEE Trans. Neural Networks* 20(1): 61–80.

Shi, H.; Pi, R.; Xu, H.; Li, Z.; Kwok, J. T.; and Zhang, T. 2019. Multi-objective Neural Architecture Search via Predictive Network Performance Optimization. *arXiv preprint arXiv:1911.09336* .

Siems, J.; Zimmer, L.; Zela, A.; Lukasik, J.; Keuper, M.; and Hutter, F. 2020. NAS-Bench-301 and the Case for Surrogate Benchmarks for Neural Architecture Search. *arXiv:2008.09777 [cs.LG]* .

Simonovsky, M.; and Komodakis, N. 2018. Graphvae: Towards generation of small graphs using variational autoencoders. In *International Conference on Artificial Neural Networks*, 412–422. Springer.

Snelson, E.; and Ghahramani, Z. 2005. Sparse Gaussian Processes using Pseudo-inputs. In *Advances in Neural Information Processing Systems 18 NIPS*, 1257–1264.

Sutskever, I.; Vinyals, O.; and Le, Q. V. 2014. Sequence to Sequence Learning with Neural Networks. In *Advances in Neural Information Processing Systems*, 3104–3112.

Szegedy, C.; Vanhoucke, V.; Ioffe, S.; Shlens, J.; and Wojna, Z. 2016. Rethinking the inception architecture for computer vision. In *CVPR*.

Tang, Y.; Wang, Y.; Xu, Y.; Chen, H.; Shi, B.; Xu, C.; Xu, C.; Tian, Q.; and Xu, C. 2020. A Semi-Supervised Assessor of Neural Architectures. In *CVPR*, 1807–1816. IEEE.

Velickovic, P.; Cucurull, G.; Casanova, A.; Romero, A.; Liò, P.; and Bengio, Y. 2018. Graph Attention Networks. In *ICLR*. OpenReview.net.

Verma, S.; and Zhang, Z. 2018. Graph Capsule Convolutional Neural Networks. *CoRR* abs/1805.08090. URL http://arxiv.org/abs/1805.08090.

White, C.; Neiswanger, W.; and Savani, Y. 2019. BANANAS: Bayesian Optimization with Neural Architectures for Neural Architecture Search. *arXiv preprint arXiv:1910.11858* .

White, C.; Nolen, S.; and Savani, Y. 2020. Local Search is State of the Art for NAS Benchmarks. *CoRR* abs/2005.02960. URL https://arxiv.org/abs/2005.02960.

Williams, R. J.; and Zipser, D. 1989. A Learning Algorithm for Continually Running Fully Recurrent Neural Networks. *Neural Comput.* 1(2): 270–280.

Wu, Z.; Pan, S.; Chen, F.; Long, G.; Zhang, C.; and Yu, P. S. 2019. A comprehensive survey on graph neural networks. *arXiv preprint arXiv:1901.00596* .

Xie, S.; Hehui, Z.; Liu, C.; and Lin, L. 2019. SNAS: stochastic neural architecture search. In *ICLR*.

Xu, D.; Zhu, Y.; Choy, C. B.; and Fei-Fei, L. 2017. Scene graph generation by iterative message passing. In *CVPR*, 5410–5419.

Xu, K.; Hu, W.; Leskovec, J.; and Jegelka, S. 2019. How Powerful are Graph Neural Networks? In *ICLR*.

Xu, K.; Li, C.; Tian, Y.; Sonobe, T.; Kawarabayashi, K.; and Jegelka, S. 2018. Representation Learning on Graphs with Jumping Knowledge Networks. In Dy, J. G.; and Krause, A., eds., *Proceedings of the 35th International Conference on Machine Learning, ICML*, volume 80 of *Proceedings of Machine Learning Research*, 5449–5458. PMLR.

Ying, C. 2019. Enumerating Unique Computational Graphs via an Iterative Graph Invariant. *CoRR* abs/1902.06192.

Ying, C.; Klein, A.; Real, E.; Christiansen, E.; Murphy, K.; and Hutter, F. 2019. Nas-bench-101: Towards reproducible neural architecture search. *arXiv preprint arXiv:1902.09635* .

Ying, Z.; You, J.; Morris, C.; Ren, X.; Hamilton, W. L.; and Leskovec, J. 2018. Hierarchical Graph Representation Learning with Differentiable Pooling. In Bengio, S.; Wallach, H. M.; Larochelle, H.; Grauman, K.; Cesa-Bianchi, N.; and Garnett, R., eds., *Advances in Neural Information Processing Systems 31*, 4805–4815.

You, J.; Ying, R.; Ren, X.; Hamilton, W. L.; and Leskovec, J. 2018. Graphrnn: Generating realistic graphs with deep auto-regressive models. *arXiv preprint arXiv:1802.08773* .

Zela, A.; Elsken, T.; Saikia, T.; Marrakchi, Y.; Brox, T.; and Hutter, F. 2020. Understanding and Robustifying Differentiable Architecture Search. In *ICLR*.

Zhang, M.; Cui, Z.; Neumann, M.; and Chen, Y. 2018. An End-to-End Deep Learning Architecture for Graph Classification. In McIlraith, S. A.; and Weinberger, K. Q., eds., *Proceedings of the Thirty-Second AAAI Conference on Artificial Intelligence*, 4438–4445. AAAI Press.

Zhang, M.; Jiang, S.; Cui, Z.; Garnett, R.; and Chen, Y. 2019. D-VAE: A Variational Autoencoder for Directed Acyclic Graphs. *arXiv preprint arXiv:1904.11088* .

Zoph, B.; and Le, Q. V. 2017. Neural Architecture Search with Reinforcement Learning. In *ICLR*.

Zoph, B.; Vasudevan, V.; Shlens, J.; and Le, Q. V. 2018. Learning transferable architectures for scalable image recognition. In *CVPR*, 8697–8710.

Appendices

In this supplement to the main paper we present some additional details and results regarding the NAS-Bench-101 and ENAS search spaces, training details of the models, proofs of the propositions and additional experiments and visualizations. Moreover, we present additional neural architecture search results using Bayesian optimization on NAS-Bench-101. Thus, we demonstrate that the proposed SVGe is well suited to find high-performing architectures in this search space. These results are only briefly mentioned in the main paper because there is no directly comparable method or baseline available from the literature evaluated on NAS-Bench-101. In addition to BO, we also evaluate a random search approach on the same SVGe triplet latent space and find promising architectures even in this simpler setup.

- Section A gives a more detailed overview about the NAS-Bench-101 dataset and the ENAS search space.
- In Section B we visualize the decoding process and include technical implementation details about our SVGe model.
- Section C contains the proofs of the proposition in the main paper.
- Section D presents additional experiments of our SVGe model and SVGe triplet.

A Details on Search Spaces

A.1 NAS-Bench-101

NAS-Bench-101 (Ying et al. 2019) is a public tabular benchmark in a restricted cell-structured search space (Zoph et al. 2018) evaluated on the CIFAR-10 image classification task (Krizhevsky 2009). The following constraints are considered: only directed-acyclic graphs are considered, the number of nodes is limited to $|V| \leq 7$ (including the input and output node) and the number of edges is limited to $|E| \leq 9$. Each node represents an operation from the operation set $\mathcal{O} = \{1 \times 1 \text{ convolution}, \ 3 \times 3 \text{ convolution}, \ 3 \times 3 \text{ max pooling}\}$. Moreover as already mentioned in Section 3.4, graphs may be isomorphic. The isomorphisms in NAS-Bench-101 are detected by a graph hashing algorithm (Ying 2019). Eventually, the NAS-Bench-101 dataset contains in total 423k unique convolutional neural architectures. These architectures are built as follows: Each cell is stacked 3 times, followed by a downsampling max-pooling layer, which halves the feature map. This pattern is repeated in total 3 times, followed by global average pooling and a dense softmax layer, which produces the output. Note that the NAS-Bench-101 search space covers ResNet-like (He et al. 2016) and InceptionNet-like (Szegedy et al. 2016) cells.

Each architecture is evaluated for $\{4, 12, 36, 108\}$ epochs and mapped to its training, test and validation quantities.

A.2 ENAS

ENAS (Pham et al. 2018) trains an RNN controller to derive new neural architectures using a weight-sharing approach, which forces all derived architectures to share the same weights. The ENAS approach consists of a macro search space and a micro search space. The macro search space contains architectures with $|V| = 12$ nodes (excluding the input and output node) and an operation set

$$\begin{aligned}\mathcal{O} = \{&3 \times 3 \text{ convolution}, \ 5 \times 5 \text{ convolution}, \\ &3 \times 3 \text{ depthwise-separable convolution}, \\ &5 \times 5 \text{ depthwise-separable convolution}, \\ &3 \times 3 \text{ max pooling}, \ 3 \times 3 \text{ average pooling}\}.\end{aligned}$$

The ENAS micro search space consists of cells with a total of $|V| = 7$ nodes (including input and output nodes), which are connected to create the neural network itself (same idea as in NAS-Bench-101). In this search space node 1 and node 2 are treated as input nodes (outputs of the two previous cells in the neural network). Each node in the DAG is a concatenation (summation of the results) of two operations. In the micro search space the 5 possible operations are $\mathcal{O} = \{3 \times 3 \text{ convolution}, \ 5 \times 5 \text{ convolution}, \text{identity}, \ 3 \times 3 \text{ max pooling}, \ 3 \times 3 \text{ average pooling}\}$. The overall neural architecture is build as follows: Each convolution cell is stacked 6 times, followed by a reduction cell. This pattern is repeated two more times, followed by a final dense softmax layer. The reduction cell is similar to the convolution cell with a spatial dimension reduction of 2 (all operations have stride 2).

In our experiments the macro search space is used with 6 layers (excluding the input and output node) and extrapolated to the original macro search space with 12 layers, without the input and output node.

B Training Details

B.1 Decoder Visualization

In Figure 1 we illustrate the decoding iterations of our SVGe model and its individual modules:

– a) visualizes the **Prop** module from Eq. (7) for the partial graph and its initial node embeddings

– b) creates a new node using module **AddNode** and selects its node type via Eq. (8)

– c) initializes the new node's embedding in the module **InitNode** Eq. (10)

– d) decides whether to add an edge to the new created node with module **AddEdges** using Eq. (11)

B.2 Details on Hyperparameters

We use similar settings to (Zhang et al. 2019) for our autoencoder models. Other hyperparamters as the learning rate are optimized using BOHB (Falkner, Klein, and Hutter 2018). All hyperparameters are summarized in Table 4. We use the model *GIN* for additional experiments in appendix D. SGD with Adam optimizer (Kingma and Ba 2015) is used for all models. Whenever the loss does not decrease for 10 epochs we multiply the learning rate with 0.1.

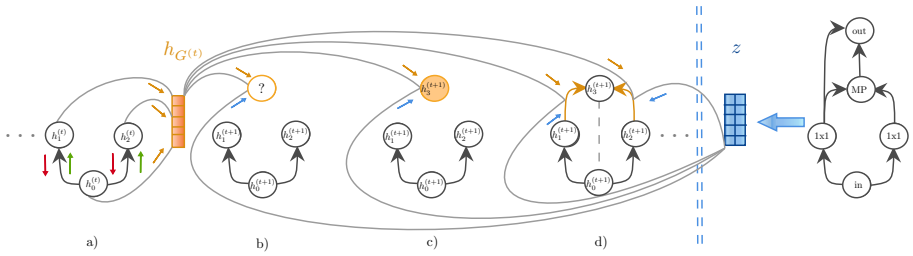

Figure 1: Illustration of a single iteration during the graph generation process. a) A decoder-level GNN propagates the node embeddings through the partially created graph and aggregates them into a summary. b) A new node is created and its node type is selected using the summary of the partially created and the original graph. c) The newly created node is initialized with a node embedding. d) A score of all edges connecting the new node is calculated and evaluated into the set of new edges.

Fine tuned SVGe For training the SVGe model jointly with the regressor for the performance prediction task, we modify the overall training loss, such that the performance prediction loss $\mathcal{L}_{\text{pred}}$ is included in the overall training loss, yielding

$$\mathcal{L} = \psi\big(\mathcal{L}_V + \mathcal{L}_E + \alpha \mathrm{D}_{\mathrm{KL}}\big) + (1-\psi)\mathcal{L}_{\text{pred}}, \tag{18}$$

where we make use of Eq. (15) for the reconstruction training of the autoencoder itself.

C Proofs

C.1 Proof of Proposition 1

Proof. Let n be the number of vertices and m the number of edges. The encoder $\phi\colon V^n \times E^m \to \mathcal{N}$ maps a graph $G = (v, e) \in V^n \times E^m$ to a normal distribution in $\mathcal{N}$, with $\mathcal{N}$ being the space of normal distribution. The decoder $\psi\colon \mathcal{N} \times V_0 \to V^n \times E^m$ maps the latent variable back to its original representation, given the initial input node $v_0 \in V$. Let $G_1 = (\bar{v}^1, \bar{e}^1), G_2 = (\bar{v}^2, \bar{e}^2) \in V^n \times E^m$ be isomorphic graphs to each other, with $\bar{v} = (v_0, \dots, v_{n-1})$. It furthermore holds by construction of all our DAGs $v_0^1 = v_0^2$. With Section 3.4 we know that our encoder ϕ maps G_1 and G_2 injectively, that is: $\phi(G_1) = \phi(G_2)$. Moreover our SVGe variational autoencoder is given by:

$$\begin{aligned} \Xi\colon V^n \times E^m &\to V^n \times E^m \\ (\bar{v}, \bar{e}) &\mapsto \psi(\phi(\bar{v}, \bar{e}), v_0). \end{aligned} \tag{19}$$

Therefore

$$\begin{aligned} \Xi(G_1) &= \Xi(\bar{v}^1, \bar{e}^1) \\ &= \psi(\phi(\bar{v}^1, \bar{e}^1), v_0^1) \\ &= \psi(\phi(\bar{v}^2, \bar{e}^2), v_0^2) \\ &= \Xi(\bar{v}^2, \bar{e}^2) \\ &= \Xi(G_2). \end{aligned}$$

□

C.2 Proof of Proposition 2

Proof. Considering any arbitrary graph G with a fixed labelling L, we can transform this graph into a graph with an upper triangular adjacency matrix without leaving its isomorphy class S_n.

This transformation goes as follows: One compares every pair of two adjacent nodes in the graph and in case that the later node appears earlier in the ordering one permutes those two nodes. After finally many steps this procedure yields a graph, whose adjacency matrix is an upper triangular matrix.

Note, that permuting two nodes v_i, v_j , with $\sigma(v_i) = v_j, \sigma(v_j) = v_i$, yields an isomorphic graph, since for each edge (i, j) in G the edge (j, i) exists in the permuted graph $\tilde{G}$, in case one permuted the nodes i and j by construction. In this argument it is enough to consider the case where only two nodes are permuted since every permutation can be written as a product of these transformations. □

D Additional Experiments

D.1 Models

We compare our SVGe and its triplet loss expansion SVGe triplet with two other baselines: D-VAE (Zhang et al. 2019) and GIN (Xu et al. 2019). D-VAE is also a graph-based autoencoder using an asynchronous message passing scheme. GIN is a graph convolution network, which also uses message passing to embed the neural architectures. In order to examine the ability of GIN in our setting, we replace our encoder with GIN and keep the decoder.

Autoencoder Abilites. Following previous work (Zhang et al. 2019; Jin, Barzilay, and Jaakkola 2018; Kusner, Paige, and Hernández-Lobato 2017), we evaluate SVGe by means of reconstruction ability, valid generation of neural architectures, the share of unique neural architectures from the valid graph set and the portion of graphs from the valid graph set, which are never seen before. For comparison reasons we evaluate these abilites on the ENAS dataset. To do so, we train the models on 90% of the dataset and test it on the 10% held-out data.

We first measure the reconstruction accuracy which describes how often our model can reconstruct the input graphs of the test set perfectly. For this purpose, after calculating the mean h_G and the variance h_G^{var} of the approximated posterior $q_\phi(\mathbf{z}|G)$ for the test set, we sample $\mathbf{z}$ from the latent

Model	Hyperparamter	Default Value
GIN	Num. node operations (ENAS)	8
	Graph hiddem dim.	56
	Num. GNN iterations layers	5
	Trainable par. ϵ	no
	VAE loss α (15)	0.005
	Batch size (ENAS)	32
	Dropout Prob.	0
	Learning rate	0.001
	Epochs	300
SVGe	Num. node operations (NAS)	5
	Num. node operations (ENAS)	8
	Node hiddem dim.	56
	Graph hiddem dim.	250
	Num. GNN iterations layers	2
	VAE loss α (15)	0.005
	Batch size (ENAS)	32
	Batch size (NAS)	128
	Dropout Prob.	0
	Learning rate	0.0001
	Epochs	300
SVGe Triplet	Triplet Loss α (16)	1.0328
	VAE Triplet loss λ (17)	0.9
	$\mathrm{d}_\kappa \leq \varepsilon$ (ENAS)	2
	$\mathrm{d}_\kappa \geq \delta$ (ENAS)	5
	Epochs	300
Regression	Loss proportion ψ	0.1
	Num. Acc. Layers	4
	Learning rate	0.001
	Batch Size	128
	Epochs	100

Table 4: Hyperparameters of the variational autoencoder and the surrogate model for performance prediction.

representation of each input graph 10 times and decode each sample again 10 times. The average portion of the decoded graphs that are identical to the input ones is then reported as the reconstruction accuracy.

The second ability we are interested in is the prior validity which quantifies how often our model is able to generate valid graphs from the SVGe prior distribution. Following (Zhang et al. 2019), we sample 1k vectors from the latent space with prior distribution $p(\mathbf{z})$ and decode each vector 10 times. The average portion of the decoded graphs that are valid is then reported as the prior validity. For a valid graph by means of the ENAS (Pham et al. 2018) search space, it has to pass the following validity checks: 1) exactly one starting point, i.e., the input node, 2) exactly one ending point, i.e., the output node, 3) there exist no nodes which do not have any predecessors, except for the input node, 4) there exist no nodes which do not have any successors, except for the output node, 5) the graphs are DAGs. The average portion of unique/novel graphs from the valid decoded graphs are reported as uniqueness/novelty.

See Table 5 for the evaluation results. We find that almost all models have a nearly perfect reconstruction accuracy, prior validity, uniqueness and novelty. GIN has the worst

Method	Accuracy	Validity	Uniqueness	Novelty
SVGe	98.97	99.69	40.22	100
SVGe Triplet	99.80	99.75	35.37	99.99
GIN	97.51	100	49.15	100
D-VAE	99.96	100	37.26	100

Table 5: Autoencoder Abilites on ENAS in %.

reconstruction accuracy for neural architectures. Since the reconstruction accuracy is very important for our tasks, we leave evaluations on GIN out of our experiments.

D.2 Performance Prediction

Figure 2 shows the predicted performance vs. the true performance of our fine tuned SVGe model from Section 4.2 for 100 sampled graphs from the training set and for 100 sampled graph from the test set on the NAS-Bench-101 test accuracies. The SVGe model is trained jointly with the regressor using 3k random samples of labelled data. We see that our model predicts the performances in an accurate and stable way.

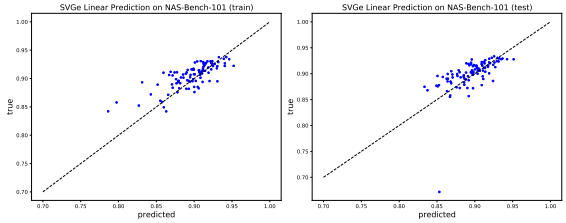

Figure 2: Performance Prediction of fine tuned SVGe on NAS-Bench-101 test accuracy of 100 sampled graphs from the training set (left) and 100 sampled graphs from the test set (right).

Dataset	Method	Top-1 Acc. (%)
NAS-Bench-101	SVGe Triplet + RS	94.72
	SVGe + BO	94.73
	SVGe Triplet + BO	94.99

Table 6: Bayesian optimization on the NAS-Bench-101 Search Space.

Bayesian Optimization on NAS-Bench-101 In addition to the experiment in Section 4.3 we also perform Bayesian optimization (BO) on the NAS-Bench-101 search space with our SVGe and SVGe triplet models. In order to cover a higher amount of graphs in the generated latent space, we sample in total 114k (30%) triplets out of the training set to train the SVGe triplet for graph reconstruction. In addition to BO, we also consider a simple random search approach on our learnt SVGe triplet space. As we can see in Table 6, SVGe's best found model achieves a validation accuracy of

94.73% when BO is used, from SVGe triplet BO even finds an architecture with an accuracy of 94.99% validation accuracy. Applying random search to the latent space allows to find an architecture with 94.72%. Thus, both our proposed smooth embedding spaces SVGe and SVGe triplet enable to find high-performing architectures - where SVGe triplet slightly improves over SVGe and even simple approaches such as random search in this latent space allow to find reasonable architectures.

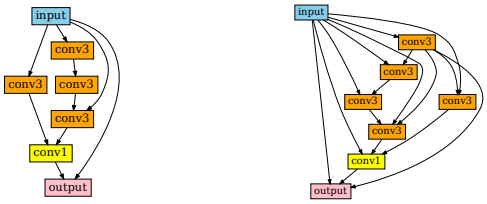

Figure 3: Visualization of the best network architectures in NAS-Bench-101 search space with respect to the validation accuracy with node length 7 (left) and node length 8 (right).

Visualization In the following we visualize the best found architectures in our extrapolation experiments, corresponding to the results in Table 2 in the main paper.

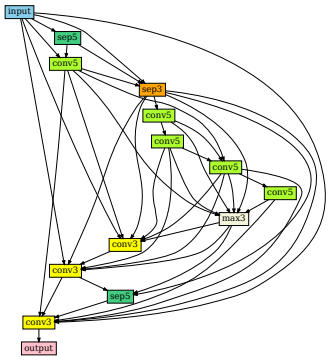

Figure 4: Visualization of the best 12-layer network architectures found by SVGe for the extrapolation task of graphs in the ENAS search space.

Figure 3 (right) visualizes the best found architecture with 8 nodes from the extrapolation experiment in Section 4.2 using the SVGe fine tuned model. We see that the predicted best performing architecture is from the superset of the best graph in the NAS-Bench-101 dataset (Figure 3 (left)).

We plot in Figure 4 the predicted best architecture with 12 layers from the ENAS macro search space.